

GLOBAL CONTEXT VISION TRANSFORMERS

Ali Hatamizadeh, Hongxu Yin, Jan Kautz, Pavlo Molchanov

NVIDIA

{ahatamizadeh, danny, jkautz, pmolchanov}@nvidia.com

ABSTRACT

We propose global context vision transformer (GC ViT), a novel architecture that enhances parameter and compute utilization for computer vision tasks. The core of the novel model are global context self-attention modules, joint with standard local self-attention, to effectively yet efficiently model both long and short-range spatial interactions, as an alternative to complex operations such as an attention masks or local windows shifting. While the local self-attention modules are responsible for modeling short-range information, the global query tokens are shared across all global self-attention modules to interact with local key and values. In addition, we address the lack of inductive bias in ViTs and improve the modeling of inter-channel dependencies by proposing a novel downampler which leverages a parameter-efficient fused inverted residual block. The proposed GC ViT achieves new state-of-the-art performance across image classification, object detection and semantic segmentation tasks. On ImageNet-1K dataset for classification, the tiny, small and base variants of GC ViT with 28M, 51M and 90M parameters achieve **83.4%**, **83.9%** and **84.4%** Top-1 accuracy, respectively, surpassing comparably-sized prior art such as CNN-based ConvNeXt and ViT-based Swin Transformer. Pre-trained GC ViT backbones in downstream tasks of object detection, instance segmentation, and semantic segmentation on MS COCO and ADE20K datasets outperform prior work consistently, sometimes by large margins. Code and pre-trained models are available at <https://github.com/NVlabs/GCViT>.

1 INTRODUCTION

During the recent years, Transformers (Vaswani et al., 2017) have achieved State-Of-The-Art (SOTA) performance in Natural Language Processing (NLP) benchmarks and became the de facto model for various tasks. A key element in the success of Transformers is the self-attention mechanism which allows for capturing contextual representations via attending to both distant and nearby tokens (Yin et al., 2021). Following this trend, Vision Transformer (ViT) (Dosovitskiy et al., 2020) proposed to utilize image patches as tokens in a monolithic architecture with minor differences comparing to encoder of the original Transformer. Despite the historic dominance of Convolutional Neural Network (CNN) in computer vision, ViT-based models have achieved SOTA or competitive performance in various computer vision tasks. In essence, the self-attention mechanism in ViT allows for learning more uniform short and long-range information (Raghu et al., 2021) in comparison to CNN. However, the monolithic architecture of ViT and quadratic computational complexity of self-attention baffle their swift application to high resolution images (Yang et al., 2021a) in which capturing multi-scale long-range information is crucial for accurate representation modeling.

Several efforts (Liu et al., 2021; Dong et al., 2022; Chu et al., 2021a; Tu et al., 2022), most notably Swin Transformer (Liu et al., 2021), have attempted to address the balance between short- and long-range spatial dependencies by proposing multi-resolution architectures in which the self-attention is computed in local windows. In this paradigm, cross-window connections such as window shifting are used for modeling the interactions across different regions. Despite the progress, the limited receptive field of local windows challenges the capability of self-attention to capture long-range information, and window-connection schemes such as shifting only cover a small neighborhood in the vicinity of each window. Subsequent efforts such as Focal Transformer (Yang et al., 2021b) attempted to address this issue by designing highly sophisticated self-attention modules with increased model complexity.

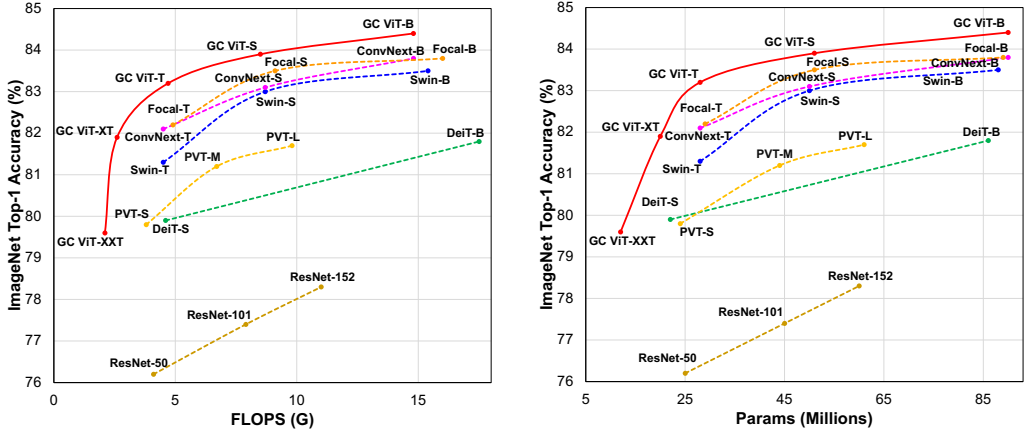


Figure 1 – Top-1 accuracy vs. model FLOPs/parameter size on ImageNet-1K dataset. GC ViT achieves new SOTA benchmarks for different model sizes as well as FLOPs, outperforming competing approaches by a significant margin. Best viewed in color.

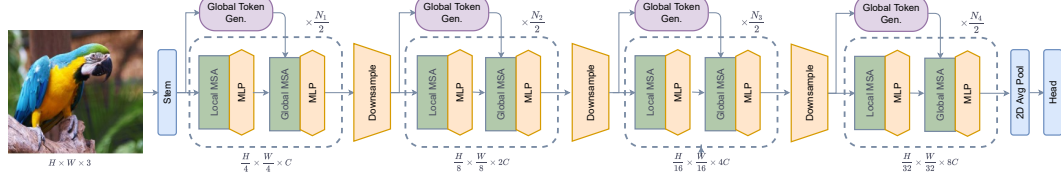


Figure 2 – Architecture of the proposed GC ViT. At each stage, a query generator extracts global query tokens which captures long-range information by interacting with local key and value representations. We use alternating blocks of local and global context self attention layers. Best viewed in color.

In this work, we introduce the Global Context (GC) ViT network to address these limitations. Specifically, we propose a hierarchical ViT architecture consisting of local and global self-attention modules. At each stage, we compute global query tokens, using a novel fused inverted residual blocks, which we refer to as modified Fused-MBConv blocks, that encompass global contextual information from different image regions. While the local self-attention modules are responsible for modeling short-range information, the global query tokens are shared across all global self-attention modules to interact with local key and value representations. The design of our proposed framework for global query generator and self-attention is intuitive and simple and can be efficiently implemented using major deep learning framework. Hence, it eliminates sophisticated and computationally expensive operations and ensures the effectiveness of self-attention when applied to high-resolution images. In addition, we propose a novel downsampling block with a parameter-efficient fused-MBConv layer to address the lack of inductive bias in ViTs and enhancing the modeling of inter-channel dependencies.

We have extensively validated the effectiveness of the proposed GC ViT using three publicly available datasets for various computer vision tasks. For image classification using ImageNet-1K dataset, GC ViT with 28M, 51M, 90M and 201M parameters, referred to as tiny, small, base and large variants, achieve new SOTA benchmarks of **83.4%**, **83.9%**, **84.4%** and **84.6%** Top-1 accuracy. Hence, GC ViT consistently outperforms both ConvNeXt (Liu et al., 2022) and Swin Transformer (Liu et al., 2021) models by a significant margin (see Fig. 1). Using a pre-trained GC ViT base backbone with a Cascade Mask RCNN (He et al., 2017) head, our model achieves a box mAP of **52.9** for object detection and a mask mAP of **45.8** for instance segmentation on the MS COCO dataset. In addition, using an UPerNet (Xiao et al., 2018) head, our model achieves a mIoU of **49.0** on ADE20K for semantic segmentation. Other variants of GC ViT with different learning capacities also demonstrate SOTA results when compared to similarly-sized models on both MS COCO and ADE20K datasets. Hence, GC ViT demonstrates great scalability for high-resolution images on various downstream tasks, validating the effectiveness of the proposed framework in capturing both short and long-range information.

The main contributions of our work are summarized as follows:

- We introduce a compute and parameter-optimized hierarchical ViT with reparametrization of the design space (*e.g.*, embedding dimension, number of heads, MLP ratio).
- We design an efficient CNN-like token generator that encodes spatial features at different resolutions for global query representations.
- We propose global query tokens that can effectively capture contextual information in an efficient manner and model both local and global interactions.
- We introduce a parameter-efficient downsampling module with modified Fused MB-Conv blocks that not only integrates inductive bias but also enables the modeling of inter-channel dependencies.
- We demonstrate new SOTA benchmarks for : (1) ImageNet classification with Pareto fronts on ImageNet-1K for model size and FLOPs (see Fig. 1), and (2) downstream tasks such as detection, instance segmentation and semantic segmentation on MS COCO and ADE20K, respectively.

2 GC ViT ARCHITECTURE

Architecture. Fig. 2 depicts the architecture of GC ViT. We propose a hierarchical framework to obtain feature representations at several resolutions (called stages) by decreasing the spatial dimensions while expanding the embedding dimension, both by factors of 2. At first, given an input image with resolution of $\mathbf{x} \in \mathbb{R}^{H \times W \times 3}$, we obtain overlapping patches by applying a 3×3 convolutional layer with a stride of 2 and appropriate padding. Then patches are projected into a C -dimensional embedding space with another 3×3 convolutional layer with stride 2. Every GC ViT stage is composed of alternating local and global self-attention modules to extract spatial features. Both operate in local windows like Swin Transformer (Liu et al., 2021), however, the global self-attention has access to global features extracted by the global token generator. The token generator is a CNN-like module that extracts features from the entire image only once at every stage. After each stage, the spatial resolution is decreased by 2 while the number of channels is increased by 2 via a downsampling block. Resulting features are passed through average pooling and linear layers to create an embedding for a downstream task.

The GC ViT architecture benefits from novel blocks such as *a downsampling operator*, *a global query generator* and *a global self-attention module* described in the next sections.

Downsampler. We leverage an idea of spatial feature contraction from CNN models that imposes locality bias and cross channel interaction while reducing dimensions. We utilize a modified Fused-MBConv block, followed by a max pooling layer with a kernel size of 3 and stride of 2 as a downsampling operator, see Fig 3. The Fused-MBConv block in our work is similar to the one in EfficientNetV2 (Tan & Le, 2021) with modifications as in

$$\begin{aligned} \hat{\mathbf{x}} &= \text{DW-Conv}_{3 \times 3}(\mathbf{x}), \\ \hat{\mathbf{x}} &= \text{GELU}(\hat{\mathbf{x}}), \\ \hat{\mathbf{x}} &= \text{SE}(\hat{\mathbf{x}}), \\ \mathbf{x} &= \text{Conv}_{1 \times 1}(\hat{\mathbf{x}}) + \mathbf{x}, \end{aligned} \tag{1}$$

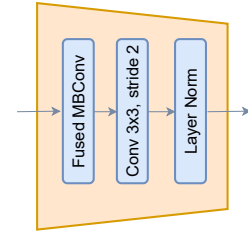


Figure 3 – Downsampling block for dimension reduction.

where SE, GELU and DW-Conv $_{3 \times 3}$ denote Squeeze and Excitation block (Hu et al., 2018), Gaussian Error Linear Unit (Hendrycks & Gimpel, 2016) and 3×3 depth-wise convolution, respectively. In our proposed architecture, the Fused-MBConv blocks provide desirable properties such as inductive bias and modeling of inter-channel dependencies. It is ablated in Table 5.

Attention. Multi-head self-attention is the the core computational operator in the GC ViT architecture, it extracts semantic information from the image. GC ViT is composed of local and global self-attention modules illustrated in Fig 4. Similar to Swin Transformer (Liu et al., 2021), we benefit from splitting the image into windows and performing local self-attention within them, this leads to linear complexity scaling with image size. The local self-attention extracts local, short-range, information and in order to facilitate long range dependencies we propose to use a novel global self attention to allow cross-patch communication with those far beyond the local window. Global self-attention attends other regions in the image via global query token that represents image embedding extracted with CNN-like module.

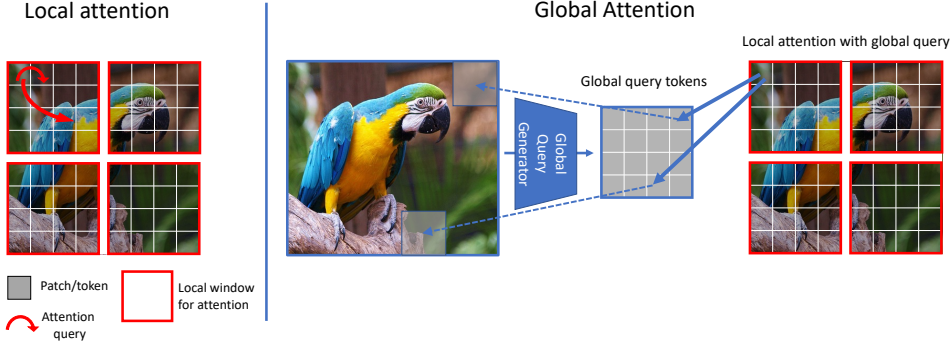


Figure 4 – Attention formulation. Local attention is computed on feature patches within local window only (left). On the other hand, the global features are extracted from the entire input features and then repeated to form global query tokens. The global query is interacted with local key and value tokens, hence allowing to capture long-range information via cross-region interaction. Best viewed in color.

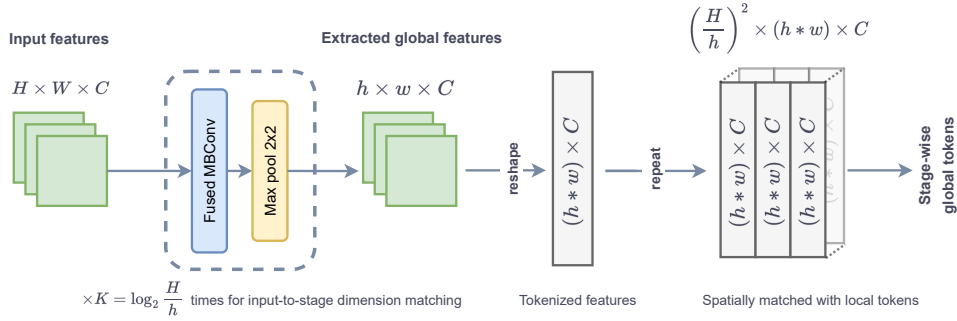


Figure 5 – Global query generator schematic diagram. It is designed to (i) transform an input feature map to the current stage of dimension H, W, C denoting height, width, and channel respectively, (ii) extract features via repeating the modified Fused MBConv block, joint with down-sampling, $\log_2 \frac{H}{h}$ times for dimension matching to local window size h (iii) output is reshaped and repeated to $(\frac{H}{h})^2$ number of local tokens that can attend to global contextual information. \star denotes merged dimensions during reshaping.

2.1 GLOBAL QUERY GENERATOR

We propose to generate global query tokens that encompass information across the entire input feature maps for interaction with local key and value feature pairs. Specifically, as shown in Fig. 5, a layer f in the generator consists of a Fused-MBConv block followed by a max pooling layer, similar to the one described in Sec. 2, and the final global query $q_{g,i}$ at stage i ($i \in \{1, 2, 3, 4\}$) of GC ViT is computed according to

$$\begin{aligned} \mathbf{x}^i &= f\text{-MBConv}(\mathbf{x}^{i-1}), \\ \mathbf{x}^i &= \text{MaxPool}(\mathbf{x}^i). \end{aligned} \quad (2)$$

These query tokens are computed once at every stage of the model and shared across all global attention layers, hence decreasing number of parameters and FLOPs and improving the generalizability. In addition, the global attention layers only learn local key and value features which will be used for interaction with global query tokens.

2.2 GLOBAL SELF-ATTENTION

Fig. 4 demonstrates the main idea behind our contribution. Local self-attention can only query patches within a local window, whereas the global attention can query different image regions while still operating within the window. At each stage, the global query component is pre-computed as described in Sec. 2.1. The global self-attention utilizes the extracted global query tokens, obtained according to Eq. 2 and shared across all blocks, to interact with the local key and value representations. In addition, GC ViT employs alternating local and global self-attention blocks to effectively capture

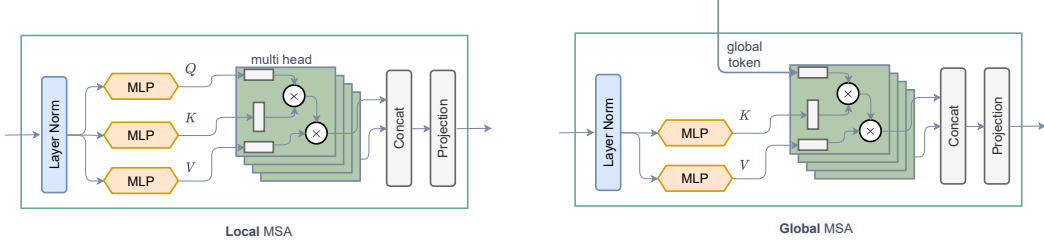


Figure 6 – Local and global attention blocks. Global attention block does not compute query vector and reuses global query computed via Global Token Generation.

both local and global spatial information. Fig. 6 illustrates the difference between local and global self-attention. The global attention query q_g has a size of $B \times C \times h \times w$, wherein B , C , h and w denote batch size, embedding dimension, local window height and width, respectively. Moreover, q_g is repeated along the batch dimension to compensate for the overall number of windows and batch size $B^* = B \times N$ where N is the number of local windows. q_g is further reshaped into multiple heads. The value and key are computed within each local window using a linear layer. The global self-attention query, key and value features are computed as follows

$$Q_g \in \mathbb{R}^{B^* \times C \times h \times w} := [q_g, \dots, q_g], q_g \in \mathbb{R}^{B \times C \times h \times w}, \quad (3)$$

$$q_g \in \mathbb{R}^{B^* \times N \times C} \xleftarrow{\text{reshape}} Q_g \in \mathbb{R}^{B^* \times C \times h \times w}, \quad (4)$$

$$k, v = g(x) \in \mathbb{R}^{B^* \times N \times C}. \quad (5)$$

Since the partitioned windows only contain local information, interaction with rich contextual information embedded in the global query tokens provides an effective way of enlarging the receptive field and attending to various regions in the input feature maps. The self-attention module is computed as in

$$\text{Attention}(q_g, k, v) = \text{Softmax}\left(\frac{q_g k}{\sqrt{d}} + b\right)v, \quad (6)$$

where d is scaling factor and b is a learnable relative position bias term. Assuming position change between $[-p+1, p-1]$ along horizontal and vertical axes, b is sampled from the grid $\hat{b} \in \mathbb{R}^{(2p-1) \times (2p-1)}$. As shown in Sec. 5, relative position bias improves the performance, especially for dense prediction downstream tasks. In Algorithm 1, we present a PyTorch-like pseudocode for computing global self-attention in GC ViT. A complexity analysis of the global self-attention is presented in the supplementary materials.

3 RELATED WORK

ViT. The ViT (Dosovitskiy et al., 2020) was first proposed as an alternative to CNNs with the advantage of enlarged receptive field, due to its self-attention layers. However, it lacked desirable properties of CNNs such as inductive biases and translation invariance and required large-scale training datasets to achieve competitive performance. Data-efficient Image Transformers (DeiT) Touvron et al. (2021b) introduced a distillation-based training strategy which significantly improved the classification accuracy. LeViT (Graham et al., 2021) proposed a hybrid model with re-designed multi-layer perceptron (MLP) and self-attention modules that are highly-optimized for fast inference. Cross-covariance Image Transformer (XCiT) (Ali et al., 2021) introduced a transposed self-attention module for

Algorithm. 1 Global Attention Pseudocode in PyTorch Style

```

# Input/output shape: (B*, N, C)
# B*: Batchsize*Num Windows; H:
# Height;
# W: Width; C: dim; q_g: Global Token
# F: Num Attention Head; N: Num Windows;
def init():
    f = nn.Linear(C, 2*C)
    softmax = nn.Softmax(dim=-1)

def forward(x, q_g):
    B*, N, C = x.shape
    B, C, h, w = q_g.shape
    kv = f(x).reshape(B*, N, 2, F, C
                      // F)
    kv = kv.permute(2, 0, 3, 1, 4)
    k, v = split(kv, (1, 1), 0)
    q_g = q_g.repeat(1, B* // B, 1, 1)
    q_g = q_g.reshape(B*, F, N, C // F
                      )
    qk = matmul(q_g, k.transpose(-2,
                                 -1))
    attn = softmax(qk)
    return matmul(attn, v).reshape(B*, N, C)

```

modeling the interactions of feature channels. Convolutional vision Transformer (CvT) (Wu et al., 2021) introduced convolutional token embedding layer and Transformer block in a hierarchical architecture to improve the efficiency and accuracy of ViTs. Conditional Position encoding Vision Transformer (CPVT) (Chu et al., 2021b) demonstrated improved performance on various tasks such as image classification and object detection by conditioning the position encoding on localized patch token. Tokens-To-Token Vision Transformer (T2T-ViT) (Yuan et al., 2021) proposed a transformation layer for aggregating adjacent tokens and establishing image prior by exploiting spatial correlations. Pyramid Vision Transformer (PVT) (Wang et al., 2021) proposed a hierarchical architecture with patch embedding at the beginning of each stage and spatial dimension reduction to improve the computational efficiency. Independently, Swin Transformers (Liu et al., 2021) also proposed a hierarchical architecture in which self-attention is computed within local windows which are shifted for region interaction. Twins Transformer (Chu et al., 2021a) proposed a spatially separable self-attention with locally-grouped and global sub-sampling modules to improve the efficiency. Focal Transformer (Yang et al., 2021b) introduced the Focal self-attention to capture long-range spatial interactions. PVT-v2 (Wang et al., 2022) improved performance and efficiency comparing to PVT (Wang et al., 2021) by introducing overlapping patch embedding, convolutional feed-forward network and linear attention.

ConvNet. Since the advent of deep learning, CNNs (Krizhevsky et al., 2012; Simonyan & Zisserman, 2014; Howard et al., 2017; He et al., 2016; Szegedy et al., 2016; Huang et al., 2017; Hu et al., 2018) have dominated computer vision benchmarks with SOTA performance. Recently, inspired by ViTs, ConvMixer (Trockman & Kolter, 2022) introduced a simple architecture with large-kernel depth-wise and point-wise convolutional layers and global pooling with competitive performance for classification. Furthermore, ConvNeXt (Liu et al., 2022) proposed modifications to the architecture of ResNet (He et al., 2016), and achieved competitive benchmarks for classification, detection and segmentation tasks.

4 EXPERIMENTS

Image classification. For image classification, we trained and tested our model on ImageNet-1K dataset (Deng et al., 2009). To allow for a fair comparison, all GC ViT variants are trained by following training configurations of previous efforts (Liu et al., 2021; Yang et al., 2021b; Chu et al., 2021a). Specifically, all models are trained on 4 nodes (32 A100 GPUs) with the AdamW (Loshchilov & Hutter, 2017) optimizer for 300 epochs with an initial learning rate of 0.001, weight decay of 0.05, cosine decay scheduler and 20 warm-up and cool-down epochs, respectively. We use total batch sizes of 4096 for GC ViT-XXT, GC ViT-XT and GC ViT-T models and 1028 for all other variants. See supplementary materials for more training details.

Object detection and semantic segmentation For object detection and instance segmentation, we trained our model on MS COCO (Lin et al., 2014) with a Mask-RCNN (He et al., 2017) head, using $\times 3$ LR schedule with an initial learning rate of 0.0001, a batch size of 16 and weight decay of 0.05. Following Liu et al. (2022), we compared against Tiny, Small and Base model variants using Cascade Mask-RCNN but only compared against Tiny variant using Mask-RCNN. For semantic segmentation, we used the ADE20K dataset (Zhou et al., 2017) with a UPerNet (Xiao et al., 2018) segmentation head. Following previous efforts, we used a random crop size of 512×512 for the input images. For fair assessment, we only compare against models with a pre-trained ImageNet-1K backbone.

4.1 CLASSIFICATION

We present the ImageNet-1K classification benchmarks in Table 1 and compare against CNN, ViT-based models across different model sizes. Our model achieves new SOTA benchmarks in all categories. Specifically, the proposed GC ViT surpasses similar-sized counterpart models by +0.5% for GC ViT-XT (82.0%) compared to T2T-ViT-14 (Yuan et al., 2021) (81.5%), +0.7% for GC ViT-T (83.4%) over CSwin-T (Dong et al., 2022) (82.7%), +0.3% for GC ViT-S (83.9%) over CSwin-S (Dong et al., 2022) (83.6%), +0.2% for GC ViT-B (84.4%) compared to CSwin-B (Dong et al., 2022) (84.2%) and +0.1% for GC ViT-L (84.6%) over CoAtNet-3 (Dai et al., 2021) (84.5%), respectively. Furthermore, as shown in Fig. 1, GC ViT models have better or comparable computational efficiency in terms of number FLOPs over the competing counterpart models.

Table 1 – Image classification benchmarks on **ImageNet-1K** dataset (Deng et al., 2009).

Method	Param (M)	FLOPs (G)	Image Size	Top-1 (%)
ResMLP-S12 (Touvron et al., 2021a)	15	3.0	224 ²	76.6
PVT-v2-B1 (Wang et al., 2022)	13	2.1	224 ²	78.7
GC ViT-XXT	12	2.1	224²	79.8
DeiT-Small/16 (Touvron et al., 2021b)	22	4.6	224 ²	79.9
T2T-ViT-14 (Yuan et al., 2021)	22	5.2	224 ²	81.5
GC ViT-XT	20	2.6	224²	82.0
ResNet50 (He et al., 2016)	25	4.1	224 ²	76.1
Swin-T (Liu et al., 2021)	29	4.5	224 ²	81.3
CoAtNet-0 (Dai et al., 2021)	25	4.2	224 ²	81.6
PVT-v2-B2 (Wang et al., 2022)	25	4.0	224 ²	82.0
ConvNeXt-T (Liu et al., 2022)	29	4.5	224 ²	82.1
Focal-T (Yang et al., 2021b)	29	4.9	224 ²	82.2
CSwin-T (Dong et al., 2022)	23	4.3	224 ²	82.7
GC ViT-T	28	4.7	224²	83.4
ResNet-101 (He et al., 2016)	44	7.9	224 ²	77.4
Swin-S (Liu et al., 2021)	50	8.7	224 ²	83.0
ConvNeXt-S (Liu et al., 2022)	50	8.7	224 ²	83.1
PVT-v2-B3 (Wang et al., 2022)	45	6.9	224 ²	83.2
CoAtNet-1 (Dai et al., 2021)	42	8.4	224 ²	83.3
Focal-S (Yang et al., 2021b)	51	9.1	224 ²	83.5
CSwin-S (Dong et al., 2022)	35	6.9	224 ²	83.6
GC ViT-S	51	8.5	224²	83.9
ResNet-152 (He et al., 2016)	60	11.6	224 ²	78.3
ViT-Base/16 (Dosovitskiy et al., 2020)	86	17.6	224 ²	77.9
DeiT-Base/16 (Touvron et al., 2021b)	86	17.6	224 ²	81.8
Swin-B (Liu et al., 2021)	88	15.4	224 ²	83.3
CoAtNet-2 (Dai et al., 2021)	42	8.4	224 ²	83.3
ConvNeXt-B (Liu et al., 2022)	89	15.4	224 ²	83.8
Focal-B (Yang et al., 2021b)	90	16.0	224 ²	83.8
PVT-v2-B5 (Wang et al., 2022)	82	11.8	224 ²	83.8
CSwin-B (Dong et al., 2022)	78	15.0	224 ²	84.2
BoTNet (Dong et al., 2022)	79	19.3	256 ²	84.2
GC ViT-B	90	14.8	224²	84.4
ConvNeXt-L (Liu et al., 2022)	198	34.4	224 ²	84.3
CoAtNet-3 (Dai et al., 2021)	168	34.7	224 ²	84.5
GC ViT-L	201	32.6	224²	84.6

Table 2 – Object detection and instance segmentation benchmarks using Mask R-CNN and Cascade Mask R-CNN on **MS COCO** dataset (Lin et al., 2014). All models employ 3× schedule.

Backbone	Param (M)	FLOPs (G)	AP ^{box}	AP ₅₀ ^{box}	AP ₇₅ ^{box}	AP ^{mask}	AP ₅₀ ^{mask}	AP ₇₅ ^{mask}
Mask-RCNN 3× schedule								
Swin-T (Liu et al., 2021)	48	267	46.0	68.1	50.3	41.6	65.1	44.9
ConvNeXt-T (Liu et al., 2022)	48	262	46.2	67.9	50.8	41.7	65.0	44.9
GC ViT-T	48	291	47.9	70.1	52.8	43.2	67.0	46.7
Cascade Mask-RCNN 3× schedule								
DeiT-Small/16 (Touvron et al., 2021b)	80	889	48.0	67.2	51.7	41.4	64.2	44.3
ResNet-50 (He et al., 2016)	82	739	46.3	64.3	50.5	40.1	61.7	43.4
Swin-T (Liu et al., 2021)	86	745	50.4	69.2	54.7	43.7	66.6	47.3
ConvNeXt-T (Liu et al., 2022)	86	741	50.4	69.1	54.8	43.7	66.5	47.3
GC ViT-T	85	770	51.6	70.4	56.1	44.6	67.8	48.3
X101-32 (Xie et al., 2017)	101	819	48.1	66.5	52.4	41.6	63.9	45.2
Swin-S (Liu et al., 2021)	107	838	51.9	70.7	56.3	45.0	68.2	48.8
ConvNeXt-S (Liu et al., 2022)	108	827	51.9	70.8	56.5	45.0	68.4	49.1
GC ViT-S	108	866	52.4	71.0	57.1	45.4	68.5	49.3
X101-64 (Xie et al., 2017)	140	972	48.3	66.4	52.3	41.7	64.0	45.1
Swin-B (Liu et al., 2021)	145	982	51.9	70.5	56.4	45.0	68.1	48.9
ConvNeXt-B (Liu et al., 2022)	146	964	52.7	71.3	57.2	45.6	68.9	49.5
GC ViT-B	146	1018	52.9	71.7	57.8	45.8	69.2	49.8

4.2 DETECTION

In Table 2, we present object detection and instance segmentation benchmarks on MS COCO dataset. Using a Mask-RCNN head, the model with pre-trained GC ViT-T (47.9/43.2) backbone outperforms counterparts with pre-trained ConvNeXt-T (Liu et al., 2022) (46.2/41.7) by +1.7 and +1.5 and Swin-T (Liu et al., 2021) (46.0/41.6) by +1.9 and +1.6 in terms of box AP and mask AP, respectively. Using a Cascade Mask-RCNN head, the models with pre-trained GC ViT-T (51.6/44.6) and GC ViT-S (52.4/45.4) backbones outperform ConvNeXt-T (Liu et al., 2022) (50.4/43.7) by +1.2 and +0.9 and ConvNeXt-S (Liu et al., 2022) (51.9/45.0) by +0.5 and +0.4 in terms of box AP and mask AP, respectively. Furthermore, the model with GC ViT-B (52.9/45.8) backbone outperforms the counterpart with ConvNeXt-B (Liu et al., 2022) (52.7/45.6) by +0.2 and +0.2 in terms of box AP and mask AP, respectively.

4.3 ADE20K SEMANTIC SEGMENTATION RESULTS

We present semantic segmentation benchmarks on ADE20K dataset in Table 3. The models using pre-trained GC ViT-T (47.0), GC ViT-S (48.3) and GC ViT-B (49.0) backbones outperform counterpart models with pre-trained Twins-SVT-S (Chu et al., 2021a) (46.2), Twins-SVT-B (Chu et al., 2021a) (47.7) and Twins-SVT-L (Chu et al., 2021a) (48.8) by +0.8, +0.6 and +0.2 in terms of mIoU, respectively. In addition, models with GC ViT backbones significantly outperform counterparts with Swin Transformer backbones, hence demonstrating the effectiveness of the global self-attention.

5 ABLATION

5.1 COMPONENT-WISE ANALYSIS

As shown in Table 4, we study the role of each component in GC ViT model for classification, detection, instance and semantic segmentation. For simplicity, we start with Swin Transformer as the base model and progressively re-design the components to demonstrate their importance in improving the performance. Firstly, we remove the window shifting and predictably observe significant performance degradation across all tasks. Changing distribution of parameters to our design improves the performance by +1.7, +2.8, +2.2 and +1.7 in terms of accuracy, box AP, mask AP and mIoU. Such reparametrization includes changing the window size, MLP ratio, number of layers to name but a few. Adding the CNN-based stem of GC ViT to the model provides additional improvements of +0.3, +0.2, +0.2 and +0.2 in terms of accuracy, box AP, mask AP and mIoU. In addition, using our proposed downsample further improves the accuracy, box AP, mask AP and mIoU by +0.4, +0.1, +0.1 and +0.3, respectively. The last two changes demonstrate the importance of convolutional inductive bias and capturing the inter-channel dependencies in our model. Finally, leveraging the proposed global self-attention improves the performance by +0.8, +0.8, +0.6 and +1.2 in terms of accuracy, box AP, mask AP and mIoU. Hence, this validates the effectiveness of the

Backbone	Param (M)	FLOPs (G)	mIoU
DeiT-Small/16 (Touvron et al., 2021b)	52	1099	44.0
Swin-T (Liu et al., 2021)	60	945	44.5
ResNet-101 (He et al., 2016)	86	1029	44.9
Twins-SVT-S (Chu et al., 2021a)	55	-	46.2
GC ViT-T	58	947	47.0
Swin-S (Liu et al., 2021)	81	1038	47.6
Twins-SVT-B (Chu et al., 2021a)	89	-	47.7
GC ViT-S	84	1163	48.3
Swin-B (Liu et al., 2021)	121	1188	48.1
Twins-SVT-L (Chu et al., 2021a)	133	-	48.8
GC ViT-B	125	1348	49.0

Table 3 – Semantic segmentation benchmarks **ADE20K** validation set with UPerNet (Xiao et al., 2018) and pre-trained ImageNet-1K backbone. All models use a crop size of 512×512 .

the counterpart with ConvNeXt-B (Liu et al., 2022) (52.7/45.6) by +0.2 and +0.2 in terms of box AP and mask AP, respectively.

	ImageNet top-1	COCO		ADE20k mIoU
		AP ^{box}	AP ^{mask}	
Swin-T	81.3	50.4	43.7	44.5
Swin-T w/o Window Shifting	80.2	47.7	41.5	43.3
+ Reparam. (window, #blocks, ratio)	81.9	50.5	43.7	45.0
+ GC ViT-T Stem	82.2	50.7	43.9	45.2
+ GC ViT-T Down-sampler	82.6	50.8	44.0	45.8
+ GC ViT-T Global Self-attention	83.4	51.6	44.6	47.0

Table 4 – Ablation study on the effectiveness of various components in GC ViT on classification, detection and segmentation performance.

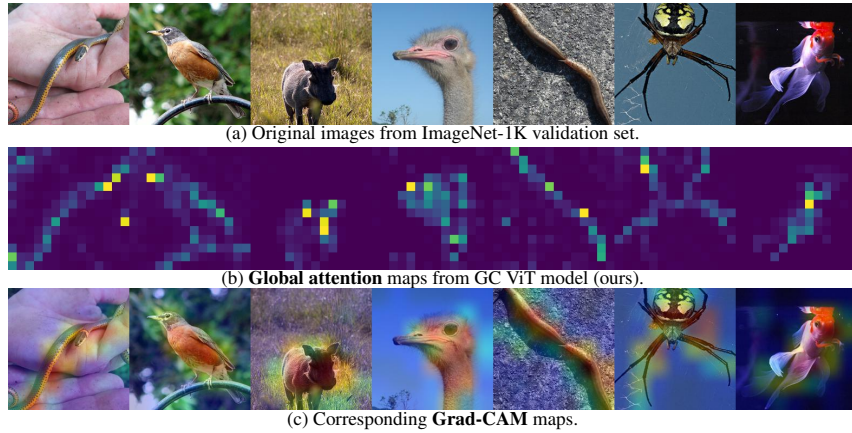


Figure 7 – Visualization of : (a) input images (b) global self-attention maps from GC ViT-T model (c) corresponding Grad-CAM attention maps. Both short and long-range spatial dependencies are captured effectively. Please see the supplementary materials for illustration of learned global query token feature maps.

proposed global self-attention, in particular for downstream tasks with high resolution images such as semantic segmentation in which modeling long-range spatial dependencies is critical.

5.2 DOWNSAMPLER DESIGN

We studied the effectiveness of various downsample blocks in Table 5. The simplest alternative to our design is a pair of convolutional and maxpooling layers. However, it results in a reduction of ImageNet Top-1 accuracy by -0.7. Patch merging is another variant which was introduced in Swin Transformers (Liu et al., 2021).

However, it reduces the accuracy by -0.5. Finally, our down-sampler which consists of a modified Fused-MBConv block and strided convolution and shows the best result. Importance of the former component is explained by the SE operation which boosts cross channel interaction while keeping number of parameters and FLOPs low. We conclude that our proposed down-sampler is essential to achieve high accuracy as it introduces convolutional inductive bias.

6 INTERPRETABILITY

To provide further insights on interpretability of the proposed global self-attention and query tokens, we demonstrate visualization of the learned attention and Grad-CAM (Selvaraju et al., 2017) maps in Fig. 7. The associated attention distributions uncovered by the global self-attention modules align with image semantics, and hence act as an informative source for local attention modules. In addition, corresponding Grad-CAM maps demonstrate accurate object localization with most intricate details.

7 CONCLUSION

We introduced a new vision transformer architecture named GC ViT that can efficiently capture global context by utilizing global query tokens and interact with local regions. Through extensive experiments we show SOTA benchmarks for image classification on ImageNet-1K dataset, surpassing CNN/ViT-based counterparts by large margin. We also consistently achieved SOTA for downstream tasks of detection, instance and semantic segmentation on MS COCO and ADE20K datasets.

REFERENCES

Alaaeldin Ali, Hugo Touvron, Mathilde Caron, Piotr Bojanowski, Matthijs Douze, Armand Joulin, Ivan Laptev, Natalia Neverova, Gabriel Synnaeve, Jakob Verbeek, et al. Xcit: Cross-covariance image transformers. *Advances in neural information processing systems*, 34, 2021.

Chun-Fu Chen, Quanfu Fan, and Rameswar Panda. Crossvit: Cross-attention multi-scale vision transformer for image classification, 2021.

Kai Chen, Jiaqi Wang, Jiangmiao Pang, Yuhang Cao, Yu Xiong, Xiaoxiao Li, Shuyang Sun, Wansen Feng, Ziwei Liu, Jiarui Xu, et al. Mmdetection: Open mmlab detection toolbox and benchmark. *arXiv preprint arXiv:1906.07155*, 2019.

Xiangxiang Chu, Zhi Tian, Yuqing Wang, Bo Zhang, Haibing Ren, Xiaolin Wei, Huaxia Xia, and Chunhua Shen. Twins: Revisiting the design of spatial attention in vision transformers. *Advances in Neural Information Processing Systems*, 34, 2021a.

Xiangxiang Chu, Zhi Tian, Bo Zhang, Xinlong Wang, Xiaolin Wei, Huaxia Xia, and Chunhua Shen. Conditional positional encodings for vision transformers. *arXiv preprint arXiv:2102.10882*, 2021b.

MMSegmentation Contributors. MMSegmentation: Openmmlab semantic segmentation toolbox and benchmark. <https://github.com/open-mmlab/mms Segmentation>, 2020.

Zihang Dai, Hanxiao Liu, Quoc V Le, and Mingxing Tan. Coatnet: Marrying convolution and attention for all data sizes. *Advances in Neural Information Processing Systems*, 34:3965–3977, 2021.

Jia Deng, Wei Dong, Richard Socher, Li-Jia Li, Kai Li, and Li Fei-Fei. Imagenet: A large-scale hierarchical image database. In *2009 IEEE conference on computer vision and pattern recognition*, pp. 248–255. Ieee, 2009.

Xiaoyi Dong, Jianmin Bao, Dongdong Chen, Weiming Zhang, Nenghai Yu, Lu Yuan, Dong Chen, and Baining Guo. Cswin transformer: A general vision transformer backbone with cross-shaped windows. In *Proceedings of the IEEE/CVF Conference on Computer Vision and Pattern Recognition*, pp. 12124–12134, 2022.

Alexey Dosovitskiy, Lucas Beyer, Alexander Kolesnikov, Dirk Weissenborn, Xiaohua Zhai, Thomas Unterthiner, Mostafa Dehghani, Matthias Minderer, Georg Heigold, Sylvain Gelly, et al. An image is worth 16x16 words: Transformers for image recognition at scale. In *International Conference on Learning Representations*, 2020.

Benjamin Graham, Alaaeldin El-Nouby, Hugo Touvron, Pierre Stock, Armand Joulin, Hervé Jégou, and Matthijs Douze. Levit: a vision transformer in convnet’s clothing for faster inference. In *Proceedings of the IEEE/CVF International Conference on Computer Vision*, pp. 12259–12269, 2021.

Kaiming He, Xiangyu Zhang, Shaoqing Ren, and Jian Sun. Deep residual learning for image recognition. In *Proceedings of the IEEE conference on computer vision and pattern recognition*, pp. 770–778, 2016.

Kaiming He, Georgia Gkioxari, Piotr Dollár, and Ross Girshick. Mask r-cnn. In *Proceedings of the IEEE international conference on computer vision*, pp. 2961–2969, 2017.

Dan Hendrycks and Kevin Gimpel. Gaussian error linear units (gelus). *arXiv preprint arXiv:1606.08415*, 2016.

Andrew G. Howard, Menglong Zhu, and Bo Chen. Mobilenets: Efficient convolutional neural networks for mobile vision applications. 2017.

Jie Hu, Li Shen, and Gang Sun. Squeeze-and-excitation networks. In *Proceedings of the IEEE conference on computer vision and pattern recognition*, pp. 7132–7141, 2018.

Gao Huang, Zhuang Liu, Laurens Van Der Maaten, and Kilian Q Weinberger. Densely connected convolutional networks. In *Proceedings of the IEEE conference on computer vision and pattern recognition*, pp. 4700–4708, 2017.

Alex Krizhevsky, Ilya Sutskever, and Geoffrey E Hinton. Imagenet classification with deep convolutional neural networks. In *Advances in neural information processing systems*, pp. 1097–1105, 2012.

Tsung-Yi Lin, Michael Maire, Serge Belongie, James Hays, Pietro Perona, Deva Ramanan, Piotr Dollár, and C Lawrence Zitnick. Microsoft COCO: Common objects in context. In *ECCV*, 2014.

Ze Liu, Yutong Lin, Yue Cao, Han Hu, Yixuan Wei, Zheng Zhang, Stephen Lin, and Baining Guo. Swin transformer: Hierarchical vision transformer using shifted windows. In *Proceedings of the IEEE/CVF International Conference on Computer Vision*, pp. 10012–10022, 2021.

Zhuang Liu, Hanzi Mao, Chao-Yuan Wu, Christoph Feichtenhofer, Trevor Darrell, and Saining Xie. A convnet for the 2020s. *arXiv preprint arXiv:2201.03545*, 2022.

Ilya Loshchilov and Frank Hutter. Decoupled weight decay regularization. *arXiv preprint arXiv:1711.05101*, 2017.

Maithra Raghu, Thomas Unterthiner, Simon Kornblith, Chiyuan Zhang, and Alexey Dosovitskiy. Do vision transformers see like convolutional neural networks? *Advances in Neural Information Processing Systems*, 34, 2021.

Ramprasaath R Selvaraju, Michael Cogswell, Abhishek Das, Ramakrishna Vedantam, Devi Parikh, and Dhruv Batra. Grad-cam: Visual explanations from deep networks via gradient-based localization. In *Proceedings of the IEEE international conference on computer vision*, pp. 618–626, 2017.

Karen Simonyan and Andrew Zisserman. Very deep convolutional networks for large-scale image recognition. *CoRR*, abs/1409.1556, 2014. URL <http://arxiv.org/abs/1409.1556>.

Christian Szegedy, Vincent Vanhoucke, Sergey Ioffe, Jon Shlens, and Zbigniew Wojna. Rethinking the inception architecture for computer vision. In *Proceedings of the IEEE conference on computer vision and pattern recognition*, pp. 2818–2826, 2016.

Mingxing Tan and Quoc Le. Efficientnetv2: Smaller models and faster training. In *International Conference on Machine Learning*, pp. 10096–10106. PMLR, 2021.

Hugo Touvron, Piotr Bojanowski, Mathilde Caron, Matthieu Cord, Alaaeldin El-Nouby, Edouard Grave, Gautier Izacard, Armand Joulin, Gabriel Synnaeve, Jakob Verbeek, et al. Resmlp: Feedforward networks for image classification with data-efficient training. *arXiv preprint arXiv:2105.03404*, 2021a.

Hugo Touvron, Matthieu Cord, Matthijs Douze, Francisco Massa, Alexandre Sablayrolles, and Hervé Jégou. Training data-efficient image transformers & distillation through attention. In *International Conference on Machine Learning*, pp. 10347–10357. PMLR, 2021b.

Asher Trockman and J Zico Kolter. Patches are all you need? *arXiv preprint arXiv:2201.09792*, 2022.

Zhengzhong Tu, Hossein Talebi, Han Zhang, Feng Yang, Peyman Milanfar, Alan Bovik, and Yinxiao Li. Maxvit: Multi-axis vision transformer. *arXiv preprint arXiv:2204.01697*, 2022.

Ashish Vaswani, Noam Shazeer, Niki Parmar, Jakob Uszkoreit, Llion Jones, Aidan N Gomez, Łukasz Kaiser, and Illia Polosukhin. Attention is all you need. In *Advances in neural information processing systems*, pp. 5998–6008, 2017.

Wenhai Wang, Enze Xie, Xiang Li, Deng-Ping Fan, Kaitao Song, Ding Liang, Tong Lu, Ping Luo, and Ling Shao. Pyramid vision transformer: A versatile backbone for dense prediction without convolutions. In *Proceedings of the IEEE/CVF International Conference on Computer Vision*, pp. 568–578, 2021.

Wenhai Wang, Enze Xie, Xiang Li, Deng-Ping Fan, Kaitao Song, Ding Liang, Tong Lu, Ping Luo, and Ling Shao. Pvt v2: Improved baselines with pyramid vision transformer. *Computational Visual Media*, 8(3):415–424, 2022.

Ross Wightman. Pytorch image models. <https://github.com/rwightman/pytorch-image-models>, 2019.

Haiping Wu, Bin Xiao, Noel Codella, Mengchen Liu, Xiyang Dai, Lu Yuan, and Lei Zhang. CvT: Introducing convolutions to vision transformers. In *Proceedings of the IEEE/CVF International Conference on Computer Vision (ICCV)*, pp. 22–31, October 2021.

Tete Xiao, Yingcheng Liu, Bolei Zhou, Yuning Jiang, and Jian Sun. Unified perceptual parsing for scene understanding. In *Proceedings of the European Conference on Computer Vision (ECCV)*, pp. 418–434, 2018.

Saining Xie, Ross Girshick, Piotr Dollár, Zhuowen Tu, and Kaiming He. Aggregated residual transformations for deep neural networks. In *Proceedings of the IEEE conference on computer vision and pattern recognition*, pp. 1492–1500, 2017.

Huanrui Yang, Hongxu Yin, Pavlo Molchanov, Hai Li, and Jan Kautz. NViT: Vision transformer compression and parameter redistribution. *arXiv preprint arXiv:2110.04869*, 2021a.

Jianwei Yang, Chunyuan Li, Pengchuan Zhang, Xiyang Dai, Bin Xiao, Lu Yuan, and Jianfeng Gao. Focal attention for long-range interactions in vision transformers. *Advances in Neural Information Processing Systems*, 34, 2021b.

Hongxu Yin, Arash Vahdat, Jose Alvarez, Arun Mallya, Jan Kautz, and Pavlo Molchanov. A-ViT: Adaptive tokens for efficient vision transformer. *arXiv preprint arXiv:2112.07658*, 2021.

Li Yuan, Yunpeng Chen, Tao Wang, Weihao Yu, Yujun Shi, Zihang Jiang, Francis EH Tay, Jiashi Feng, and Shuicheng Yan. Tokens-to-token ViT: Training vision transformers from scratch on imagenet. In *ICCV*, 2021.

Bolei Zhou, Hang Zhao, Xavier Puig, Sanja Fidler, Adela Barriuso, and Antonio Torralba. Scene parsing through ade20k dataset. In *Proceedings of the IEEE conference on computer vision and pattern recognition*, pp. 633–641, 2017.

A APPENDIX

B GC ViT MODEL CONFIGURATIONS

GC ViT model configurations are presented in Table S.1 describing the choice of internal hyper parameters to obtain models with various compute load and parameter number.

	Output Size (Downs. Rate)	GC ViT-XT	GC ViT-T	GC ViT-S	GC ViT-B
Stem	128×128 (2×)	Conv, C:64, S:2, LN	Conv, C:64, S:2, LN	Conv, C:96, S:2, LN	Conv, C:128, S:2, LN
		[F-MBConv C:64] × 1	[F-MBConv C:64] × 1	[F-MBConv C:96] × 1	[F-MBConv C:128] × 1
Stage 1	56×56 (4×)	Conv, C:128, S:2, LN	Conv, C:128, S:2, LN	Conv, C:192, S:2, LN	Conv, C:256, S:2, LN
		[LG-SA, C:64, head:2] × 3, F-MBConv, C:128	[LG-SA, C:64, head:2] × 3, F-MBConv, C:128	[LG-SA, C:96, head:3] × 3, F-MBConv, C:192	[LG-SA, C:128, head:4] × 3, F-MBConv, C:256
Stage 2	28×28 (8×)	Conv, C:256, S:2, LN	Conv, C:256, S:2, LN	Conv, C:384, S:2, LN	Conv, C:512, S:2, LN
		[LG-SA, C:64, head:4] × 4, F-MBConv, C:256	[LG-SA, C:64, head:4] × 4, F-MBConv, C:256	[LG-SA, C:96, head:6] × 4, F-MBConv, C:384	[LG-SA, C:128, head:8] × 4, F-MBConv, C:512
Stage 3	14×14 (16×)	Conv, C:512, S:2, LN	Conv, C:512, S:2, LN	Conv, C:768, S:2, LN	Conv, C:1024, S:2, LN
		[LG-SA, C:64, head:8] × 6, F-MBConv, C:512	[LG-SA, C:64, head:8] × 19, F-MBConv, C:512	[LG-SA, C:96, head:12] × 19, F-MBConv, C:768	[LG-SA, C:128, head:16] × 19, F-MBConv, C:1024
Stage 4	7×7 (32×)	Conv, C:1024, S:2, LN	Conv, C:1024, S:2, LN	Conv, C:1536, S:2, LN	Conv, C:2048, S:2, LN
		[LG-SA, C:64, head:16] × 5, F-MBConv, C:1024	[LG-SA, C:64, head:16] × 5, F-MBConv, C:1024	[LG-SA, C:96, head:24] × 5, F-MBConv, C:1536	[LG-SA, C:128, head:32] × 5, F-MBConv, C:2048

Table S.1 – Architecture configurations for GC ViT. LG-SA and Conv denotes local, global self-attention and 3×3 convolutional layer, respectively. GC ViT-XT, GC ViT-T, GC ViT-S and GC ViT-B denote XTiny, Tiny, Small and Base variants, respectively.

C ABLATION

C.1 GLOBAL QUERY

We performed ablation studies to validate the effectiveness of the proposed global query. Using the same architecture, instead of global query, we compute: (1) global key and value features and interact them with local query (2) global value features and interact it with local query and key. As shown in Table S.2, replacing global query may significantly impact the performance for image segmentation and downstream tasks such as object detection, instance segmentation and semantic segmentation.

	ImageNet top-1	COCO		ADE20k mIoU
		AP _{box}	AP _{mask}	
w. Global KV	82.5	49.9	41.3	44.6
w. Global V	82.7	50.8	42.4	45.1
GC ViT-T	83.4	51.6	44.6	47.0

Table S.2 – Ablation study on the effectiveness of the proposed global query for classification, detection and segmentation.

C.2 EMA AND BATCH SIZE

We also used used Exponential Moving Averages (EMA) and observed slight improvement in terms of ImageNet TOp-1 accuracy. Furthermore, the performance of the model across different batch sizes were stable as we did not observe significant changes. Table S.3 demonstrates the effect of EMA and batch size on the accuracy of a GCViT-T model.

Model	Local Batch Size	Global Batch Size	EMA	Top-1
GC ViT-T	32	1024	No	83.37
GC ViT-T	128	4096	No	83.38
GC ViT-T	32	1024	Yes	83.39
GC ViT-T	128	4096	Yes	83.40

Table S.3 – Ablation study on the effect of EMA and batch size on GC ViT-T ImageNet Top-1 accuracy.

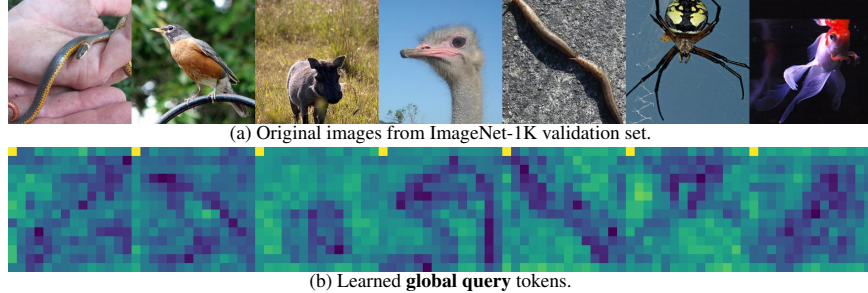


Figure S.1 – Visualization of : (a) input images (b) learned global query token feature maps.

D INTERPRETABILITY

In Fig. S.1, we illustrate the learned global query token maps and demonstrate their effectiveness in capturing long-range contextual representations from different image regions.

E TRAINING DETAILS

For image classification, GC ViT models were trained using four computational nodes with 32 NVIDIA A100 GPUs. The total training batch size is 1024 (32 per GPU) for GC ViT-S, GC ViT-B, GC ViT-L and 4096 (128 per GPU) for GC ViT-XXT, GC ViT-XT and GC ViT-T. On average, each model required 32 hours of training with the specified hyper-parameters as indicated in the paper. All classification models were trained using the `timm` package (Wightman, 2019). Object detection and instance segmentation models as well as semantic segmentation models were trained using one computational node with 8 NVIDIA A40 GPUs using a total batch size of 16, hence a batch size of 2 per GPU. Detection and instance segmentation models were trained using `mmdetection` (Chen et al., 2019) package and on average required 56 hours of training. Semantic segmentation models were trained using `mmsegmentation` (Contributors, 2020) package, and on average required 34 hours of training.

F COMPLEXITY ANALYSIS

Given an input feature map of $x \in \mathcal{R}^{H \times W \times C}$ at each stage with a window size of $h \times w$, the computational complexity of GC ViT is as follows

$$\mathcal{O}(\text{GC ViT}) = 2HW(2C^2 + hwC), \quad (7)$$

The efficient design of global query token generator and other components allows to maintain a similar computational complexity in comparison to Swin Transformer Liu et al. (2021) while being able to capture long-range information and achieve better higher accuracy for classification and downstream tasks such as detection and segmentation.

G IMAGENET CLASSIFICATION BENCHMARKS

In Table S.4, we provide a comprehensive benchmark in terms of Top-1 accuracy for the models that are only trained on ImageNet-1K (Deng et al., 2009) dataset, and without additional data.

Table S.4 – Image classification benchmarks on **ImageNet-1K** dataset (Deng et al., 2009).

Method	Param (M)	FLOPs (G)	Image Size	Top-1 (%)
ResMLP-S12 (Touvron et al., 2021a)	15	3.0	224 ²	76.6
PVT-v2-B1 (Wang et al., 2022)	13	2.1	224 ²	78.7
GC ViT-XXT	12	2.1	224²	79.8
DeiT-Small/16 (Touvron et al., 2021b)	22	4.6	224 ²	79.9
T2T-ViT-14 (Yuan et al., 2021)	22	5.2	224 ²	81.5
GC ViT-XT	20	2.6	224²	82.0
ResNet50 (He et al., 2016)	25	4.1	224 ²	76.1
PVT-Small (Wang et al., 2021)	24	3.8	224 ²	79.8
Twins-PCPVT-S (Chu et al., 2021a)	24	3.8	224 ²	81.2
Swin-T (Liu et al., 2021)	29	4.5	224 ²	81.3
CoAtNet-0 (Dai et al., 2021)	25	4.2	224 ²	81.6
Twins-SVT-S (Chu et al., 2021a)	24	2.9	224 ²	81.7
PVT-v2-B2 (Wang et al., 2022)	25	4.0	224 ²	82.0
ConvNeXt-T (Liu et al., 2022)	29	4.5	224 ²	82.1
Focal-T (Yang et al., 2021b)	29	4.9	224 ²	82.2
CSwin-T (Dong et al., 2022)	23	4.3	224 ²	82.7
GC ViT-T	28	4.7	224²	83.4
ResNet-101 (He et al., 2016)	44	7.9	224 ²	77.4
ResMLP-S24 (Touvron et al., 2021a)	30	6.0	224 ²	79.3
PVT-Medium (Wang et al., 2021)	44	6.7	224 ²	81.2
T2T-ViT-19 (Yuan et al., 2021)	39	8.9	224 ²	81.9
Twins-PCPVT-B (Chu et al., 2021a)	44	6.7	224 ²	82.7
Swin-S (Liu et al., 2021)	50	8.7	224 ²	83.0
Twins-SVT-B (Chu et al., 2021a)	56	8.6	224 ²	83.2
ConvNeXt-S (Liu et al., 2022)	50	8.7	224 ²	83.1
PVT-v2-B3 (Wang et al., 2022)	45	6.9	224 ²	83.2
CoAtNet-1 (Dai et al., 2021)	42	8.4	224 ²	83.3
Focal-S (Yang et al., 2021b)	51	9.1	224 ²	83.5
CSwin-S (Dong et al., 2022)	35	6.9	224 ²	83.6
GC ViT-S	51	8.5	224²	83.9
ResNet-152 (He et al., 2016)	60	11.6	224 ²	78.3
ViT-Base/16 (Dosovitskiy et al., 2020)	86	17.6	224 ²	77.9
ResMLP-B24 (Touvron et al., 2021a)	116	23.0	224 ²	81.0
PVT-Large (Wang et al., 2021)	61	9.8	224 ²	81.7
DeiT-Base/16 (Touvron et al., 2021b)	86	17.6	224 ²	81.8
CrossViT-B (Chen et al., 2021)	104	21.2	224 ²	82.2
T2T-ViT-24 (Yuan et al., 2021)	64	14.1	224 ²	82.3
CPVT-B (Chu et al., 2021b)	88	17.6	224 ²	82.3
Twins-PCPVT-L (Chu et al., 2021a)	61	9.8	224 ²	83.1
Swin-B (Liu et al., 2021)	88	15.4	224 ²	83.3
CoAtNet-2 (Dai et al., 2021)	42	8.4	224 ²	83.3
PVT-v2-B4 (Wang et al., 2022)	62	10.1	224 ²	83.6
Twins-SVT-L (Chu et al., 2021a)	99	15.1	224 ²	83.7
ConvNeXt-B (Liu et al., 2022)	89	15.4	224 ²	83.8
Focal-B (Yang et al., 2021b)	90	16.0	224 ²	83.8
PVT-v2-B5 (Wang et al., 2022)	82	11.8	224 ²	83.8
CSwin-B (Dong et al., 2022)	78	15.0	224 ²	84.2
BoTNet (Dong et al., 2022)	79	19.3	256 ²	84.2
GC ViT-B	90	14.8	224²	84.4
ConvNeXt-L (Liu et al., 2022)	198	34.4	224 ²	84.3
CoAtNet-3 (Dai et al., 2021)	168	34.7	224 ²	84.5
GC ViT-L	201	32.6	224²	84.6